QCES LNM Lab Report:
Ice Melt Induced Flow in a Stably Stratified Fluid
(Experiment D.3)

Unique ID: 135826

Due: 18/12/2024

1 Introduction

Anthropogenic climate change is very likely to be associated with current ice sheet melt and sea level rise, which will continue to increase associated risks for at least centuries to come (IPCC 2023). Ice sheet mass loss is driven by the sum of frontal ablation and climatic-basal balance, with frontal ablation in marine terminating glaciers being the dominant driver of loss in Greenland and both halves of Antarctica (Kochtitzky et al. 2023; Dømgaard et al. 2024; Cook et al. 2014). Submarine melting provides a control on frontal ablation of marine terminating glaciers both directly and by affecting the rate of calving (O'Leary and Christoffersen 2013; Ma and Bassis 2019).

Some work suggests that this melting has been historically underestimated (Sutherland et al. 2019). The velocity of dissolution/melting is dependent on the salinity, which has further effects on the turbulence near the interface and the speed of melt (Kerr and McConnochie 2015). Additionally, the profile of melting and the dynamics of flow are dependent on the stratification (Yang et al. 2023).

The experiment conducted in this report reproduces the work of Huppert and Turner 1980 by measuring at lab scales the melting of a vertically oriented ice block in a stable stratification. This experiment allows us to view a complex system of double-diffusive processes that have utility in the modeling and parametrisation of ice melting.

1.1 Aims

In this report, we aim to:

- Qualitatively observe the flow phenomena associated with ice melt in a stratified fluid.
- Observe and parametrise the evolution of flow structures in the fluid.
- Compare the experimental results with theoretical models.

2 Theory

Water's density varies with salinity, temperature, pressure and state. In terms of particle theory, this can be explained by added higher molar mass, higher or lower required volume of particle motion (for both temperature and pressure), and expanded volume due to the structure of H-bonds for state. Modeling this quantitatively, however, is significantly less straightforward.

2.1 Density Variation of Water

The current standard used to calculate the density of water is the Thermodynamic Equation of State for Seawater 2010 (TEOS-10 2010). TEOS-10 uses a thermodynamic function known as the Gibbs function to constrain the properties of seawater. Taking the inverse of the pressure derivative of the Gibbs function returns the density.

The Gibbs function is defined thermodynamically in Equation 1 (Feistel 2008).

$$g \equiv u + Pv - Ts \tag{1}$$

$$\text{where } \mathrm{d}u = -P\mathrm{d}v + T\mathrm{d}S_A \tag{2}$$

$$\therefore \mathrm{d}g = v\mathrm{d}P - s\mathrm{d}T + \mu\mathrm{d}S_A \tag{3}$$

$$\text{where } s(T,P) = -\left.\frac{\partial g}{\partial T}\right|_P \tag{4}$$

$$\text{and } \mu(S_A,T,P) = \left.\frac{\partial g}{\partial S_A}\right|_{T,P} \tag{5}$$

Where:

g = Gibbs function

T = temperature

u = internal energy

s = specific entropy

P = pressure

S_A = absolute salinity

v = specific volume

μ = chemical potential

The expression for density derived from this is approximated polynomially to avoid the computational difficulties of taking derivatives of the Gibbs function. TEOS-10 uses a 75-term polynomial approximation to compute this, which is nonlinear in both temperature and salinity, as well as having a pressure dependence (Roquet et al. 2015).

By taking a linear approximation of the Gibbs function for small perturbations of the temperature and salinity, and a constant pressure, the change in specific volume can be approximated for small changes Δ in S and T as Equation 6. The derivation shown gives α and β to agree with TEOS-10 (2010) and the result agrees with the previous UNESCO model (Dalziel 2024; Sanderson, Dietrich, and Stilgoe 2002).

$$\text{From (3)} : v + \Delta v = \frac{\partial g}{\partial P} = v - \frac{\partial s}{\partial P}\Delta T + \frac{\partial \mu}{\partial P}\Delta S_A \tag{6}$$

$$\frac{v + \Delta v}{v} = (1 + \alpha\Delta T - \beta\Delta S_A)$$

$$\frac{\Delta v}{v} = +\alpha\Delta T - \beta\Delta S_A$$

$$\rho = \frac{1}{v} \tag{7}$$

$$\rho + \Delta\rho \simeq \frac{1}{v} + \Delta v \times \frac{\mathrm{d}\rho}{\mathrm{d}v} \tag{8}$$

$$\rho + \Delta\rho = \rho - \rho\frac{\Delta v}{v}$$

$$\rho + \Delta\rho = \boxed{\rho(1 - \alpha\Delta T + \beta\Delta S)} \tag{9}$$

Where:

ρ = density at reference temperature (T) and salinity (S)

$\Delta\rho$ = density difference with temperature and salinity perturbations ($\Delta T, \Delta S$)

α = thermal expansion coefficient ($\frac{\partial^2 g/\partial T\partial P}{\partial g/\partial P}$)

β = salinity contraction coefficient ($\frac{\partial^2 g/\partial S\partial P}{\partial g/\partial P}$)

The values of α and β used for this experiment were the derivatives taken from TEOS-10 (2010), at standard pressure $P = 101\,325\,\text{Pa}, T = 20\,^\circ\text{C}, S = 0\,\text{PSU}$, our reference density is, therefore, $\rho = 998.2\,\text{kg}\,\text{m}^{-3}$. The error between this approximation and TEOS-10 (2010) is shown in Figure 1.

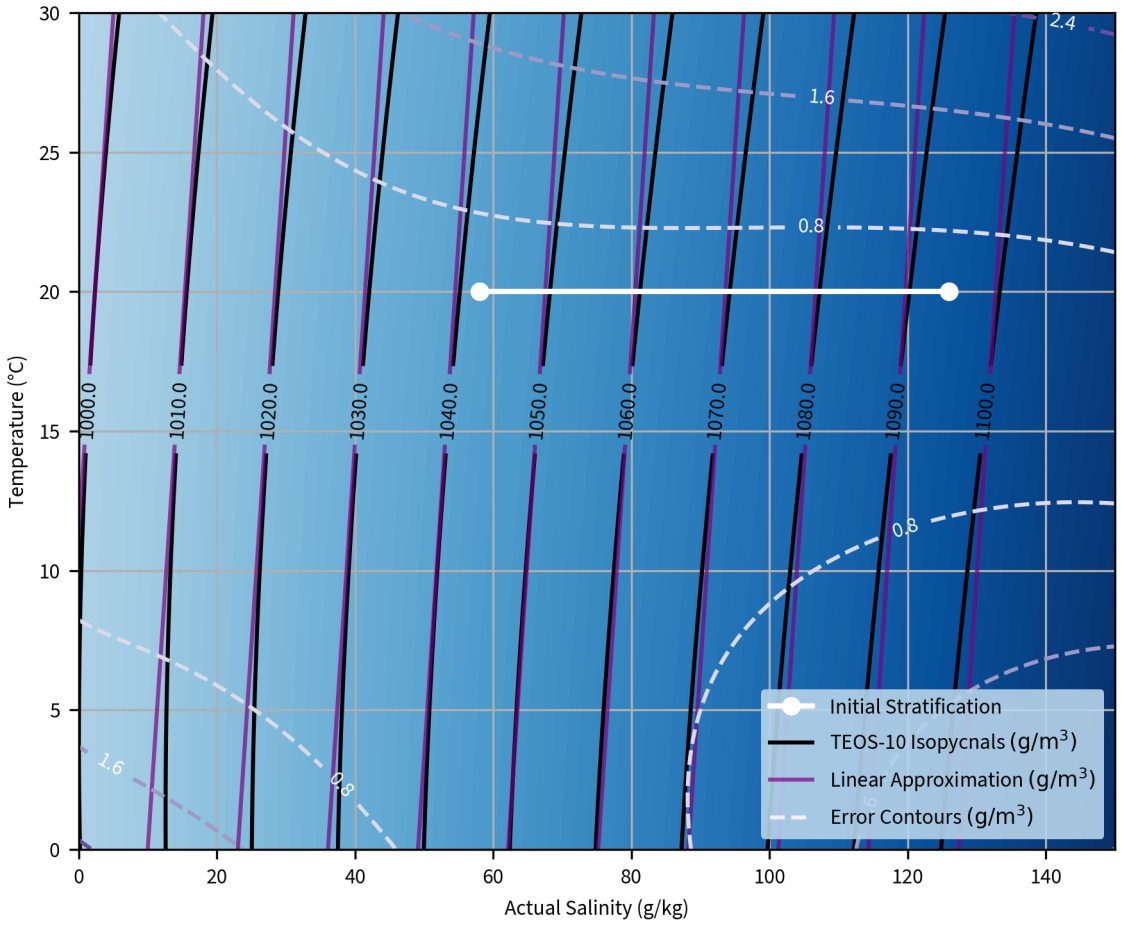

Figure 1: Comparison of water density with exact model and local approximation. Background colour represents actual (TEOS) density. Errors in our linear approximation are insignificant within our domains.

2.2 Empirical Models for Layer Formation

The vertical length scale of the layer formation has been modeled as Equation 10 (Dalziel 2024; Huppert and Turner 1980), which was supported by simulation (Yang et al. 2023).

$$h = 0.65(\rho(T_w, S_\infty) - \rho(T_\infty, S_\infty))/\frac{\mathrm{d}\rho}{\mathrm{d}z} \tag{10}$$

$$h = 0.65(\rho\alpha\Delta T)/\frac{\mathrm{d}\rho}{\mathrm{d}z} \tag{11}$$

3 Method

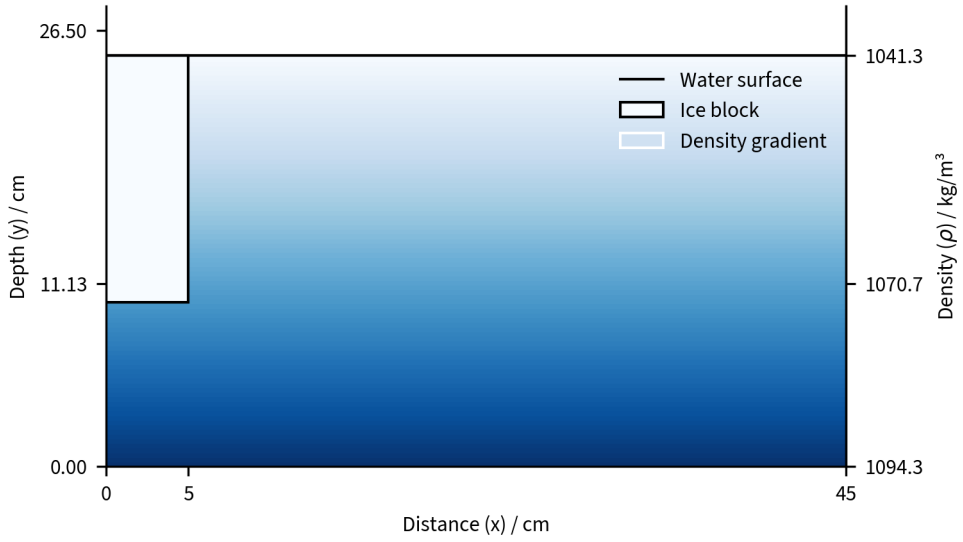

Figure 2: Layout of experimental setup with dimensions. Axis labels marked were directly measured.

3.1 Stratification Setup

The stratification was constructed using the fixed-drain, top-down, double-bucket method (Dalziel 2024; Fortuin 1960; Bader and Morgan 1962; Oster and Yamamoto 1963), with $\rho \simeq 998.2\,\mathrm{kg\,m^{-3}}$ fresh and $\rho = 1100\,\mathrm{kg\,m^{-3}}$ saline water as the two end-members. A sponge float was used to reduce turbulence and mixing of the less dense incoming fluid. (Economidou and Hunt 2009).

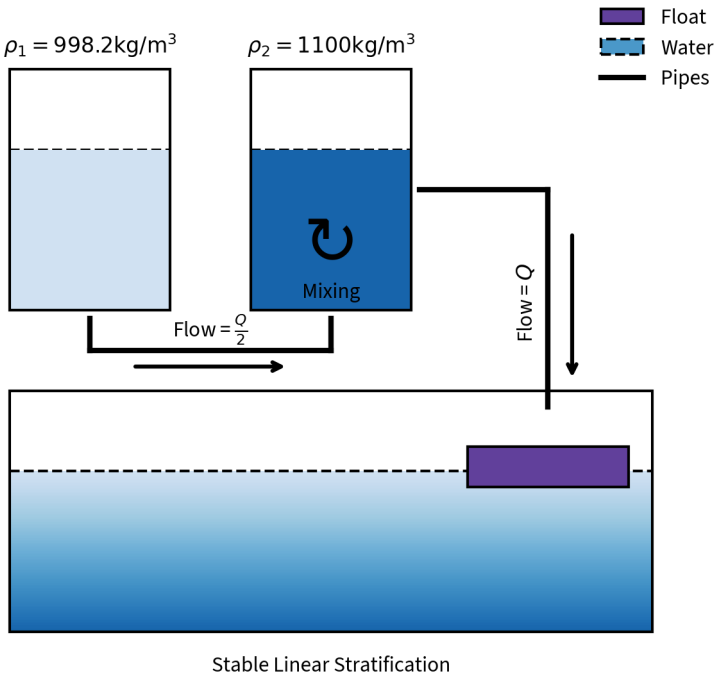

Figure 3: Schematic of the double-bucket method. Only one pump is required, on the right pipe, as gravity maintains the other pipe's flow. Colour reflects the density of the fluid.

The salinity was measured at three points (free surface: $y = 0\,\text{cm}$, half-way depth: $y = 13.25\,\text{cm}$, and bottom: $y = 26.5\,\text{cm}$), using a refractometer. The density gradient calculated from those measurements is plotted on Figure 2.

3.2 Measurements and Experimental Errors

The ice block was dyed with blue food dye. Density was measured with a HANNA HI96801 digital refractometer. Shadowgraph (Braeuer 2015) and colour images were recorded using an iPhone 14 Pro at 30fps, and detailed measurements of this video were conducted by stabilising and performing pitch correction in DaVinci Resolve. Lab measurements used a metre stick with millimetre markings and a Samsung Galaxy Z Fold 3's stopwatch feature. Methylene blue dye was added at later times to visualise flow. The precision of those instruments is tabulated in Table 1.

Instrument	Error (Unit)	Typical Value (Unit)	Error (%)
HI96801 Refractometer	±0.2 Brix	12.4 Brix	16%
Video Length Measurements	±0.1 cm	22.5 cm	0.4%
Video Time Measurements	±0.03 s	1200 s	0.0025%
Metre Stick	±0.1 cm	22.5 cm	0.4%
Stopwatch	±0.01 s	1200 s	0.0008%

Table 1: Maximum error of instruments from the maximum of scale precision and reported instrument error (where applicable). Percent error is calculated using a mean value from the dataset in Appendix A (Hanna 2017).

4 Results

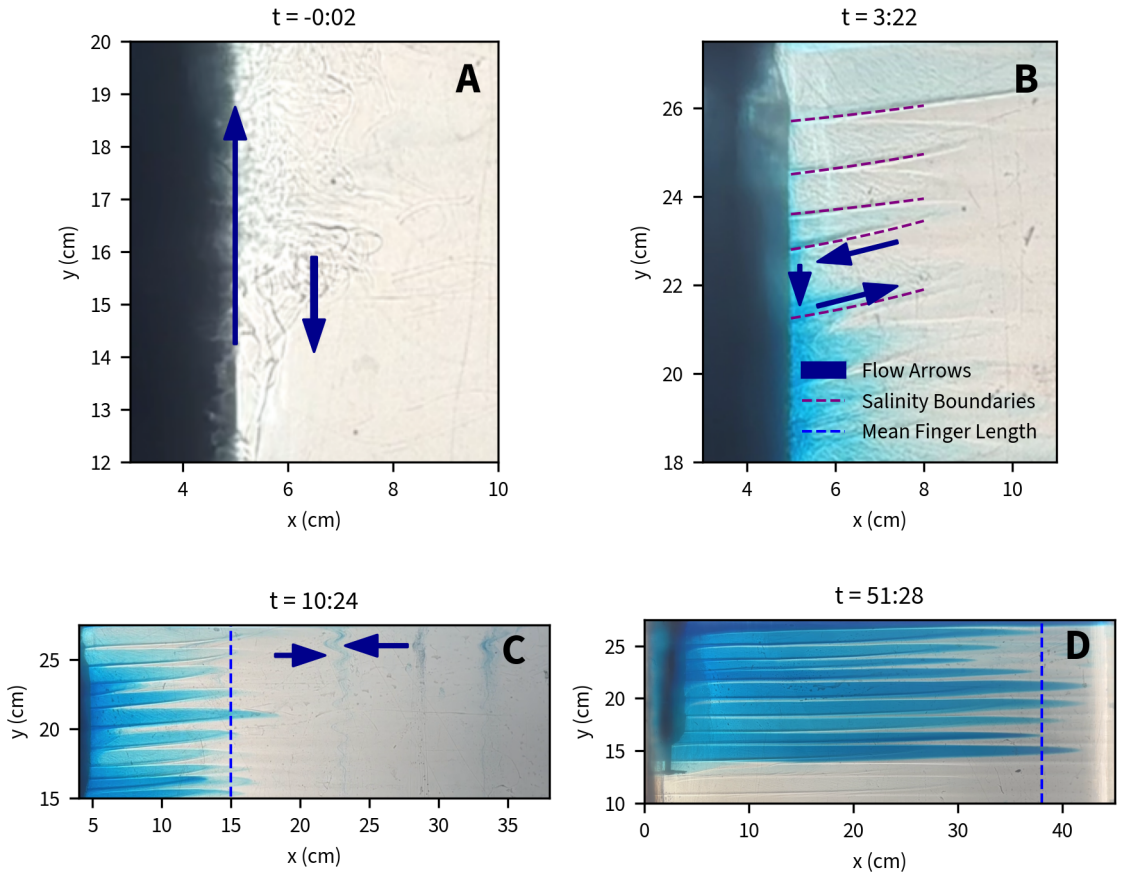

Figure 4: Shadowgraph images of the ice block at different times. $t = 0$ is the moment the ice block reaches its final position. Arrows are qualitatively related to flow speed.

These results are largely based on shadowgraph lines and dye movement. The shadowgraph records density differences. Note that the majority of dyed water is not melt, as the volume is many times that of the meltwater. Instead, the dye is diffusing with temperature, qualitiatively indicating the "affected" region of the tank.

4.1 Early Time

As the block was inserted Figure 4 (A), the shadowgraph images showed two significant movement patterns. The first was the upwelling meltwater, which begins by forming a thin turbulent plume directly in front of the ice block. This meltwater has both a significantly lower temperature and salinity than the ambient water, and therefore rises quickly to the top of the tank.

The second feature was the sinking of diffusively cooled ambient tank water. At early times, this was most noticeable underneath the ice block, but there was some downwelling directly by the meltwater plume as the turbulence generated mixing and heat diffusion, which acts much faster than saline diffusion.

4.2 Structure Formation

As the flow stabilises and the affected region becomes larger, two further effects become pronounced. The sinking, due to a negative temperature anomaly eventually becomes balanced by the density gradient from the ambient water drawn from the far-field tank, and sharp boundaries in salinity

are formed. These then concentrate horizontal movement into "finger-like" structures as the sinking water must, by mass conservation, go outwards instead of crossing these isopycnals. This can be seen in the dyed water, as this has come into close contact with the ice block. Furthermore, this outwards flow induces an intake of water from the positive x direction, setting up convective cells. These have a vertical length scale measured with a mean of 1.28 cm ± 0.13.

Noteably these sharp shadowgraph boundaries curve upwards, due to warming of the water as it moves outwards. This in turn makes it less dense, and so it moves upwards in the stratification in maintaining neutral buoyancy.

4.3 Structure Evolution

The "finger" density boundary structures diffuse outwards with a rate shown in Figure 5.

Stable flow in this regime was shown in the movement of methylene blue streaks in Figure 4 (C). As time progresses, the diffusion of salt means the curve in the salinity boundaries weakens. Figure 4 (D).

At late times, you can see the meltwater layer as thick, heavily dyed and lying on top of the original stratification, due to its near zero salinity. It also is clear that the thin turbulent layer by the ice surface is continually supplied and flows upward, as this is how the melt reaches the surface.

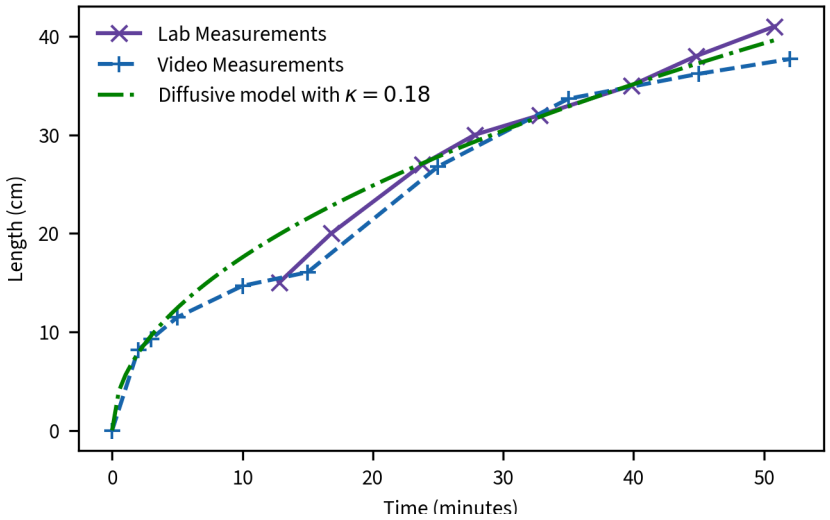

Figure 5: Mean length of the finger structures. Measurements taken in the lab were supplemented by data from the recorded video.

5 Discussion

5.1 Overall Fluid Motion

The overall motion of fluid in the tank can be summarised. The ice block is melting, creating a thin plume of rising meltwater with low density thanks to its near zero salinity. The mixing of this cold melt and conduction from the ice causes cooling of several parcels in the stratification which fall until they re-establish neutral buoyancy, forming boundaries of flow. This movement draws in far-field water, inducing horizontal flow all the way across the tank. The outward flow along these boundaries entrains pollutants (dye) from the ice. These boundaries curve upwards as temperature diffusion lowers the water along the boundary's density.

These finger structures diffuse forward with time according to a diffusivity of $0.18\,\mathrm{m^2\,s^{-1}}$ and their structures stabilise with time. Eventually the curving boundaries become more flat thanks to the diffusion of salt.

5.2 Comparison with Theory

5.2.1 Vertical Scale

The length scale of the finger structures is calculated according to Equation 10, using the mean density and temperature difference at $t = 0$, (i.e. $\Delta T = 20\,^{\circ}\mathrm{C}$), as well as α from Equation 2.1. This gives us a scale of $h_{\text{theory}} = 1.38\,\mathrm{cm}$. This is within 2σ of our measured mean of $1.20\,\mathrm{cm} \pm 0.13$, and our measured mean increases with time, probably as the experiment did not have enough time to reach the steady state that is predicted in (Huppert and Turner 1980; Yang et al. 2023).

The vertical scale does vary with time, but this variation is not well predicted by our assumptions which are all constant. The vertical depth of the whole tank and therefore the density gradient does actually change across the experiment due to the injection of meltwater, which may explain some of this variation, but the temperature gradient decreases, which I would expect to dominate and lower the scale with time. If we were to reconstruct the equation from Huppert and Turner (1980), we would produce a constant $c = 0.57 \pm 0.06$, which is again within 2σ of the previous value of 0.65.

The increasing residuals should be further investigated.

5.2.2 Horizontal Speed

Molecular diffusion of heat should dominate the horizontal speed of the finger structures. The timescale for heat diffusion is shown in Equation 12. This is much larger for 10 cm than the measured time, which is due to the effects of turbulent and convective mixing effects. Molecular diffusion of salt is even slower than this. The timescale is almost right for the first centimetre; at early times, diffusion dominates, whereas mixing structures then become more important.

A better estimate might come from an estimate of the volume within 1cm of the ice block multiplied by the diffusive timescale to get an estimate for the flow generated by cooling that volume. Our measurements of the time scale do scale roughly as length squared, so an eddy diffusive model may be accurate. From our data, a diffusivity of 0.18 seems to fit reasonably well as in Figure 5.

$$\tau = \frac{h^2}{\kappa} = \frac{(10\,\mathrm{cm})^2}{1.43 \times 10^{-7}\,\mathrm{m^2\,s^{-1}}} = 19\,\mathrm{h} \tag{12}$$

5.3 Effects in the Environment

The results suggesting that eddy diffusivity are important further imply that turbulent mixing is dominant process for the transfer of heat to the ice from the ocean. This means that understanding the turbulence in submarine glacial termination environments will allow us to understand how fast the circulation driven will respond, and how that circulation will change given a changing stratification, temperature gradient or geometry. Some work suggests that atmospheric warming will affect the submarine melting through the behaviour of plumes (Slater and Straneo 2022).

6 Conclusion

The overall motion of the fluid is dominated by two processes, a thin turbulent layer of upwelling meltwater, and the concentration of density boundaries by the balance of cooling and stratification into "finger" structures, which curve upwards due to temperature diffusion. These structures advect horizontally with an eddy diffusive timescale with $\kappa = 0.18\,\mathrm{m^2\,s^{-1}}$. We measured their characteristic vertical length scale of $h = 1.20\,\mathrm{cm} \pm 0.13$, and calculated a constant for 10 of $c = 0.57 \pm 0.06$, and found reasonable agreement with previous work. (Huppert and Turner 1980; Kerr and McConnochie 2015; Yang et al. 2023).

6.1 Future Work

It would be interesting to repeat this trial with more measurements of temperature and a more detailed measurement of the stratification as it varies with time, so we could determine why our

length scale is time variant. Additionally, a taller piece of ice and a wider tank would allow us to avoid boundary effects.

References

Bader, Hermann and H.E. Morgan (1962). "Gradient elution of phosphatides from silicic acid column". In: *Biochimica et Biophysica Acta* 57.1, pp. 562–568. ISSN: 0006-3002. DOI: https://doi.org/10.1016/0006-3002(62)91164-2. URL: https://www.sciencedirect.com/science/article/pii/0006300262911642.

Braeuer, Andreas (2015). "Chapter 4 - Shadowgraph and Schlieren Techniques". In: *In situ Spectroscopic Techniques at High Pressure*. Ed. by Andreas Braeuer. Vol. 7. Supercritical Fluid Science and Technology. Elsevier, pp. 283–312. DOI: https://doi.org/10.1016/B978-0-444-63422-1.00004-3. URL: https://www.sciencedirect.com/science/article/pii/B9780444634221000043.

Cook, A.J. et al. (2014). "A new Antarctic Peninsula glacier basin inventory and observed area changes since the 1940s". In: *Antarctic Science* 26.6, pp. 614–624. DOI: 10.1017/S0954102014000200.

Dalziel, Stuart B. (2024). *Laboratory Notes: MPhil/Part III in Quantitative Climate and Environmental Sciences*. URL: https://www.climate.cam.ac.uk/education/teaching-materials.

Dømgaard, Mads et al. (May 2024). "Early aerial expedition photos reveal 85 years of glacier growth and stability in East Antarctica". In: *Nature Communications* 15.1, p. 4466. ISSN: 2041-1723. DOI: 10.1038/s41467-024-48886-x. URL: https://doi.org/10.1038/s41467-024-48886-x.

Economidou, M. and G. R. Hunt (Mar. 2009). "Density stratified environments: the double-tank method". In: *Experiments in Fluids* 46.3, pp. 453–466. ISSN: 1432-1114. DOI: 10.1007/s00348-008-0571-8. URL: https://doi.org/10.1007/s00348-008-0571-8.

Feistel, Rainer (2008). "A Gibbs function for seawater thermodynamics for -6 to 80C and salinity up to 120gkg-1". In: *Deep Sea Research Part I: Oceanographic Research Papers* 55.12, pp. 1639–1671. ISSN: 0967-0637. DOI: https://doi.org/10.1016/j.dsr.2008.07.004. URL: https://www.sciencedirect.com/science/article/pii/S0967063708001489.

Fortuin, J. M. H. (1960). "Theory and application of two supplementary methods of constructing density gradient columns". In: *Journal of Polymer Science* 44.144, pp. 505–515. DOI: 10.1002/pol.1960.1204414421.

Hanna (2017). *HI 96801, Refractometer for Sucrose Measurements Instruction Manual*. URL: https://www.hannainst.com/hubfs/product-manuals/MAN96801_04_17.pdf?hsLang=en.

Huppert, Herbert E. and J. Stewart Turner (1980). "Ice blocks melting into a salinity gradient". In: *Journal of Fluid Mechanics* 100.2, pp. 367–384. DOI: 10.1017/S0022112080001206.

IPCC (2023). *Climate Change 2023: Synthesis Report.* Contribution of Working Groups I, II, III to the Sixth Assessment Report of the Intergovernmental Panel on Climate Change [Core Writing Team, H. Lee, and J. Romero (eds.)]. IPCC, Geneva, Switzerland, pp. 35–115. DOI: 10.59327/IPCC/AR6-9789291691647.. URL: https://www.ipcc.ch/report/ar6/syr/.

Kerr, Ross C. and Craig D. McConnochie (2015). "Dissolution of a vertical solid surface by turbulent compositional convection". In: *Journal of Fluid Mechanics* 765, pp. 211–228. DOI: 10.1017/jfm.2014.722.

Kochtitzky, William et al. (2023). "Closing Greenland's Mass Balance: Frontal Ablation of Every Greenlandic Glacier From 2000 to 2020". In: *Geophysical Research Letters* 50.17. e2023GL104095 2023GL104095, e2023GL104095. DOI: https://doi.org/10.1029/2023GL104095. eprint: https://agupubs.onlinelibrary.wiley.com/doi/pdf/10.1029/2023GL104095. URL: https://agupubs.onlinelibrary.wiley.com/doi/abs/10.1029/2023GL104095.

Ma, Yue and Jeremy N. Bassis (2019). "The Effect of Submarine Melting on Calving From Marine Terminating Glaciers". In: *Journal of Geophysical Research: Earth Surface* 124.2, pp. 334–346. DOI: https://doi.org/10.1029/2018JF004820. eprint: https://agupubs.onlinelibrary.wiley.com/doi/pdf/10.1029/2018JF004820. URL: https://agupubs.onlinelibrary.wiley.com/doi/abs/10.1029/2018JF004820.

O'Leary, M. and P. Christoffersen (2013). "Calving on tidewater glaciers amplified by submarine frontal melting". In: *The Cryosphere* 7.1, pp. 119–128. DOI: 10.5194/tc-7-119-2013. URL: https://tc.copernicus.org/articles/7/119/2013/.

Oster, Gerald and Masahide Yamamoto (1963). "Density Gradient Techniques." In: *Chemical Reviews* 63.3, pp. 257–268. DOI: 10.1021/cr60223a003. eprint: https://doi.org/10.1021/cr60223a003. URL: https://doi.org/10.1021/cr60223a003.

Roquet, F. et al. (2015). "Accurate polynomial expressions for the density and specific volume of seawater using the TEOS-10 standard". In: *Ocean Modelling* 90, pp. 29–43. ISSN: 1463-5003. DOI: https://doi.org/10.1016/j.ocemod.2015.04.002. URL: https://www.sciencedirect.com/science/article/pii/S1463500315000566.

Sanderson, Brian, David Dietrich, and Neil Stilgoe (2002). "A numerically effective calculation of sea water density". In: *Marine Models* 2.1, pp. 19–34. ISSN: 1369-9350. DOI: https://doi.org/10.1016/S1369-9350(01)00002-5. URL: https://www.sciencedirect.com/science/article/pii/S1369935001000025.

Slater, D. A. and F. Straneo (Oct. 2022). "Submarine melting of glaciers in Greenland amplified by atmospheric warming". In: *Nature Geoscience* 15.10, pp. 794–799. ISSN: 1752-0908. DOI: 10.1038/s41561-022-01035-9. URL: https://doi.org/10.1038/s41561-022-01035-9.

Sutherland, D. A. et al. (2019). "Direct observations of submarine melt and subsurface geometry at a tidewater glacier". In: *Science* 365.6451, pp. 369–374. DOI: 10.1126/science.aax3528. eprint: https://www.science.org/doi/pdf/10.1126/science.aax3528. URL: https://www.science.org/doi/abs/10.1126/science.aax3528.

TEOS-10 (2010). *The International Thermodynamic Equation Of Seawater - 2010: Calculation and Use of Thermodynamic Properties*. Intergovernmental Oceanographic Commission, Manuals and Guides No. 56, UNESCO. URL: https://www.teos-10.org/pubs/TEOS-10_Manual.pdf.

Yang, Rui et al. (2023). "Ice melting in salty water: layering and non-monotonic dependence on the mean salinity". In: *Journal of Fluid Mechanics* 969, R2. DOI: 10.1017/jfm.2023.582.

Appendices

A Data

All lengths are in centimetres, times in minutes. nstrat and lstrat are the number and vertical length of all the stratification layers.

Lab Measurements, Video Measurements:

time	length
0	15
4	20
11	27
15	30
20	32
27	35
32	38
38	41

,

time	length	nstrat	lstrat
0	0	0	0
2	8.20	14	11.8
3	9.28	14	11.63
5	11.48	14	13.51
10	14.67	12	13.50
15	16.05	12	13.52
25	26.77	14	17.36
35	33.66	15	19.06
45	36.19	14	19.10
52	37.69	13	17.53